Academic Journal of Earth Sciences
ISSN: 2960-0162
DOI: https://doi.org/10.61784/ajes3011

MINERALOGICAL AND GEOCHEMICAL CHARACTERISTICS OF THE BIOTITE MONZOGRANITE AND ASSOCIATED ION-ADSORPTION RARE EARTH ELEMENT DEPOSIT AT BAN NAM AO, HOUAPHANH PROVINCE, LAOS

PeiYuan Sun*, JiaYun Zhou
Chinese Academy of Geological Sciences, Chengdu 610041, Sichuan, China.
Corresponding Author: PeiYuan Sun, Email: 1367179639@qq.com

Abstract: Ion-adsorption-type rare earth element (REE) deposits represent a dominant resource in China. In-depth research on these deposits is crucial for enhancing the security of China's critical metal resources. Laos, a key country along the "Belt and Road" initiative, is rich in mineral resources, with significant discoveries including iron, gold, copper, lead-zinc, bauxite, and potash. In recent years, Laos has made substantial progress in REE exploration, identifying numerous deposits with development potential, among which REEs constitute a vital component. This study focuses on the weathering crust profile and fresh biotite monzogranite from the Ban Nam Ao ion-adsorption-type REE deposit in Houaphanh Province, Laos. Whole-rock major and trace element analyses, mineral composition determinations, and zircon U-Pb geochronology were conducted to elucidate the geochemical characteristics of the parent rock, its mineralogical features, and the enrichment behavior of REEs within the weathering crust. The zircon U-Pb age of the biotite monzogranite is (246.5 ± 0.59) Ma. The Ban Nam Ao granite exhibits high SiO_2 (average 69.07%), Al_2O_3, and K_2O contents, with an average Rittmann index of 1.5, classifying it as a calc-alkaline magmatic rock. The biotite monzogranite is characterized by high total REE concentrations and abundant easily decomposable REE-bearing minerals, making it an excellent source for ion-adsorption-type REE mineralization. Within the weathering profile, REE concentrations are generally elevated from the topsoil to the completely weathered layer and semi-weathered layer, with the highest REE enrichment observed at the transition zone between the completely and semi-weathered layers.
Keywords: Biotite monzogranite; Ion-adsorption-type REE deposit; Petrogenesis; Ban Nam Ao

1 INTRODUCTION

Rare Earth Elements (REEs), belonging to Group IIIB of the periodic table, comprise the lanthanide series (La-Lu, atomic numbers 57-71) and yttrium (Y), totaling 16 metallic elements. Based on geochemical classification, La-Eu are categorized as light rare earth elements (LREEs), while Gd-Lu and Y constitute heavy rare earth elements (HREEs). Owing to their unique 4f electron configurations, REEs exhibit exceptional optical, magnetic, and electrical properties, and are widely distributed in alkaline rocks, carbonatites, granites, alkaline ultramafic rocks, and associated deposits . These characteristics render REEs critical raw materials for modern high-tech industries, driving global demand[1].

Ion-adsorption-type REE deposits, the predominant source of HREEs, are of significant scientific interest due to their distinctive mineralization mechanisms and resource characteristics. These deposits form through weathering and leaching of parent rocks (e.g., granites, tuffs), with REEs adsorbed as cations onto clay minerals, layered aluminosilicates, and colloidal materials. Diverse protoliths, including granites (> 95%), volcanic rocks, migmatites, carbonatites, and alkaline rocks, contribute to their formation, among which biotite/muscovite granites and monzogranites dominate (> 90%)[2]. Studies indicate that REEs primarily exist in ion-exchangeable forms adsorbed onto clay minerals within weathering profiles, with mineralization strongly influenced by the geochemistry of accessory minerals (e.g., monazite, xenotime, apatite, allanite, titanite) in parent rocks .

Globally, REE supply chains exhibit pronounced geopolitical implications. China’s ion-adsorption-type deposits, enriched in HREEs, represent a strategic resource. Deciphering their mineralization mechanisms provides theoretical guidance for exploration and sustainable utilization, offering insights for mining practices[2-3] .

Against this backdrop, this study investigates the Ban Nam Ao ion-adsorption-type REE deposit in Houaphanh Province, Laos, through whole-rock major/trace element analysis and zircon U-Pb geochronology of weathering profiles and biotite monzogranite. The objectives are to: (1) characterize the geochemical signatures of the parent rock, and (2) elucidate REE enrichment mechanisms in the weathering crust. The findings will advance the understanding of ion-adsorption-type REE mineralization in Southeast Asia and support regional exploration strategies, while contributing to global REE resource security and China’s strategic decision-making.

2 REGIONAL GEOLOGICAL BACKGROUND

Northern Laos constitutes the southern extension of the Yunnan "Sanjiang" orogenic belt in China, which can be divided into two first-order tectonic units: the Tanggula-Changdu-Simeng-Huayxay fold belt and the Gangdese-Nyainqentanglha-Phongsaly fold belt. These are further subdivided into four second-order tectonic units from west to

© By the Author(s) 2025, under the CC BY-NC-ND license (http://creativecommons.org/licenses/by-nc-nd/4.0).

east: the Huayxay Variscan-Indosinian island arc belt with NNE-trending structural lineaments, the Phongsaly Mesozoic depression belt with NE-trending structures, the Luang Prabang Variscan fold belt featuring NNE-trending lineaments, and the Truong Son Variscan fold belt characterized by NW-trending structures. The Huayxay belt represents the southern continuation of the Changning-Menglian fold belt within the Sanjiang orogenic zone, while the remaining three units correspond to the Lanping-Simao depression belt and Mojiang-Lüchun fold belt in Yunnan . These tectonic belts exhibit markedly different structural trends, reflecting distinct evolutionary pathways of the regional geology.

Northern Laos features well-developed stratigraphic sequences dominated by Upper Paleozoic and Mesozoic formations, which collectively constitute over 80% of the exposed strata, with the remainder consisting of Precambrian and Cenozoic units. The Paleozoic succession, mainly distributed in northern and eastern regions, includes Cambrian weakly metamorphosed limestones, shales, sandstones and conglomerates, as well as Ordovician-Permian marine carbonates, sandstones and argillaceous rocks. Mesozoic strata, particularly well-exposed in the Sam Neua area, comprise Middle-Upper Triassic marine limestones, sandstones and siltstones, overlain by Late Triassic-Cretaceous paralic to continental sandstones and conglomerates, culminating in Late Cretaceous red argillaceous siltstones, fine-grained sandstones and evaporite sequences.

Precambrian basement rocks outcrop in northern and western Laos as medium-to high-grade metamorphic complexes whose protoliths were terrigenous clastic sediments interbedded with intermediate-mafic volcanic rocks. Although lacking direct stratigraphic or geochronological evidence, these are provisionally classified as Proterozoic. Cenozoic deposits fill intermontane basins in northern Laos, consisting primarily of sandstones, argillaceous rocks and minor marls, with occasional lignite seams .

The region's stratigraphic architecture reflects multiple phases of marine transgression-regression cycles and subsequent continental deposition, with the Paleozoic marine sequences recording the evolution of the Paleo-Tethys Ocean, while the Mesozoic units document the transition to terrestrial conditions during the Indosinian orogeny. Of particular note is the widespread distribution of Late Cretaceous evaporites, suggesting arid paleoclimatic conditions prior to the Cenozoic basin development. This stratigraphic framework provides critical constraints for understanding the tectonic evolution of the eastern Tethyan domain and the mineralization potential of northern Laos.

Laos exhibits predominantly Paleozoic and Cenozoic magmatic activity, with rock compositions ranging from ultramafic to acidic, though basic to intermediate-acidic varieties predominate. Volcanic activity is primarily recorded in Carboniferous-Permian and Triassic strata, with the former dominated by basic volcanic rocks and the latter characterized by intermediate-acidic volcanics. Intrusive rocks are mainly distributed in the northwestern and southeastern regions, consisting predominantly of biotite monzogranite emplaced during the Late Paleozoic to Mesozoic. Additionally, Cenozoic rift-related basaltic flows and undated ultramafic to basic intrusions are locally exposed.

The magmatic evolution of Laos reflects its tectonic development, with distinct spatial-temporal distribution patterns across different structural units. The Luang Prabang Fold Belt (Pak Lay-Luang Prabang zone) and northwestern Huayxay Fold Belt contain extensive Permian andesitic-dacitic volcanics, representing products of Permian arc magmatism. In contrast, the eastern Truong Son Variscan Fold Belt records multiple magmatic episodes since the Caledonian, exhibiting widespread and prolonged magmatism with complex pulses.

Paleozoic eugeosynclinal zones experienced polyphase intermediate-acidic to basic intrusions. During Early to Middle Indosinian stages, extension along the Nam Jiang fault system generated thick geosynclinal deposits comprising rhyolites, andesites and keratophyres. By Late Indosinian, this fault evolved into an island arc system, producing voluminous syn- to post-collisional hybridized calc-alkaline granitoids and diorites with hypabyssal to subvolcanic facies. Himalayan orogeny triggered renewed uplift and folding, accompanied by intrusions of granites and alkaline monzonites. These magmatic-volcanic processes provided essential material sources for subsequent mineralization events.

3 SAMPLING AND ANALYTICAL METHODS

The study area is located in the Ban Nam Ao region of Houaphanh Province, northeastern Laos, where the biotite monzogranite exhibits coarse-grained euhedral granular texture composed predominantly of plagioclase (30%), orthoclase (30%), quartz (25%), and biotite (10%), with accessory minerals including muscovite, pyrite, and apatite. The weathering crust profile in Ban Nam Ao is vertically divided into topsoil (0-2 m), completely weathered layer (2-19 m), and semi-weathered layer (19-28 m). The reddish-brown topsoil consists mainly of clay minerals and quartz grains, while the pinkish to grayish-white completely weathered layer contains clay minerals, quartz, and feldspar. The brownish-gray semi-weathered layer shows well-developed fractures and is dominated by granitic rock fragments.

For this study, one fresh biotite monzogranite sample was collected for zircon U-Pb geochronological analysis, and fifteen granite samples were obtained for whole-rock major and trace element (including REE) analyses. A systematic sampling approach was adopted for the weathering profile, collecting 19 samples at 2-meter intervals: 1 topsoil sample (0-2 m), 11 completely weathered layer samples (2-19 m), and 7 semi-weathered layer samples (19-28 m). All samples were carefully selected to represent the characteristic weathering products at each horizon, ensuring proper documentation of the vertical geochemical variations within the weathering profile. Sample preparation followed standard procedures for geochemical analysis, including crushing, grinding, and quartering to obtain representative aliquots for different analytical techniques.

Zircon U-Pb isotopic dating was conducted at Beijing Createch Testing Technology Co., Ltd., employing a combined

system of Analytik Jena PQMS inductively coupled plasma mass spectrometer (ICP-MS) and RESOLution 193nm excimer laser ablation system. The analytical protocol utilized a laser beam diameter of 24μm with 5Hz repetition rate and energy density maintained at approximately 5J/cm², using high-purity helium as the carrier gas. Prior to formal analysis, the international zircon standard GJ-1 was used to optimize instrument parameters and ensure optimal system performance[4]. Single-spot ablation mode was adopted for measurements, with GJ-1 serving as the primary reference material for age calibration. For trace element quantification, NIST 610 was used as the external standard while Zr content in zircon was applied as the internal standard. To ensure data quality, GJ-1 standard was re-analyzed after every 10 unknown samples for process monitoring, with Plesovice standard periodically measured to evaluate instrumental stability. The obtained Plesovice age of 337.0±1.2 Ma showed excellent agreement with its recommended value (337.13±0.37 Ma), confirming data reliability. Data reduction was performed using LADR_1.1.07 software, where no common lead correction was applied to analyses with $^{206}Pb/^{204}Pb$ ratios >1000, while analyses showing ^{204}Pb anomalies were discarded. Final age calculations and concordia diagrams were generated using Isoplot 4.15, following established analytical procedures[4] .

4 ANALYTICAL RESULTS

4.1 Zircon U-Pb Geochronology of the Granite

The analyzed zircon grains are colorless, transparent, and exhibit euhedral prismatic morphology with relatively consistent aspect ratios averaging 3:1. Grain sizes range from 100 to 200 μm. Cathodoluminescence (CL) imaging reveals characteristic magmatic oscillatory zoning with alternating bright and dark banding patterns , showing no evidence of inherited cores. These features confirm the predominantly magmatic origin of the zircons. A total of 15 analytical spots were measured using LA-ICP-MS (Table 1).

Table 1 Zircon U-Pb Geochronological Data of the Ban Nam Ao Biotite Monzogranite

Sample	Pb（ppm）	Th（ppm）	U（ppm）	Th/U	Pb/U	$^{207}Pb/^{206}Pb$	Age（Ma）	Age（Ma）	Age（Ma）
YS2-1	29.31	96.13	581.32	0.0523	0.3055	0.0426	297.3	270.7	268.9
YS2-2	32.21	114.3	803.59	0.0522	0.2798	0.0386	294.8	250.5	244.1
YS2-3	19.61	47.92	440.11	0.0161	0.2722	0.039	288.7	244.5	246.6
YS2-4	47.99	175.97	1081.74	0.0111	0.265	0.0382	242.9	240.3	241.5
YS2-5	17.13	130.02	359.49	0.052	0.2764	0.0388	253.3	247.8	245.2
YS2-6	32.93	248.15	1174.24	0.0016	0.2765	0.0391	238.4	247.9	247
YS2-7	48.29	334.59	1004.6	0.0007	0.2693	0.0387	227.6	242.2	244.9
YS2-8	29	300.28	581.66	0.0053	0.27	0.0391	209.7	242.7	247.2
YS2-9	38.3	149.52	1388.18	0.0321	0.2669	0.0402	287.3	256.1	253.9
YS2-10	29.36	60.32	666.38	0.0111	0.2722	0.0387	242.8	244.7	244.7
YS2-11	47.66	61.01	1020.28	0.0008	0.2748	0.0389	231.2	246.1	246.3
YS2-12	44.55	380.35	926.26	0.0316	0.2754	0.0387	265.2	247	244.5
YS2-13	32.95	66.02	797.93	0.005	0.2751	0.04	194	246.8	252.8
YS2-14	52.48	361.34	568.23	0.0062	0.3409	0.0469	457.5	438.5	433
YS2-15	21.97	52.08	457.45	0.0118	0.2925	0.0408	274.7	260.5	257.8

With the exception of one analytical spot yielding a $^{206}Pb/^{238}U$ age of 433.0 ± 4.9 Ma, the remaining fourteen spots display tightly clustered $^{206}Pb/^{238}U$ ages ranging from 241.5 to 268.9 Ma with high concordance. The concordia age derived from $^{206}Pb/^{238}U$-$^{207}Pb/^{235}U$ systematics is 246.5 ± 0.59 Ma (MSWD of concordance = 0.87; Fig. 1A), while the weighted mean $^{206}Pb/^{238}U$ age is 246.5 ± 1.2 Ma (Fig. 1B). The remarkable consistency between these two age determinations indicates that 246.5 Ma represents the crystallization age of the ore-bearing biotite monzogranite associated with the Ban Nam Ao ion-adsorption REE deposit in Houaphanh Province, Laos, corresponding to Triassic Indosinian magmatism[5].

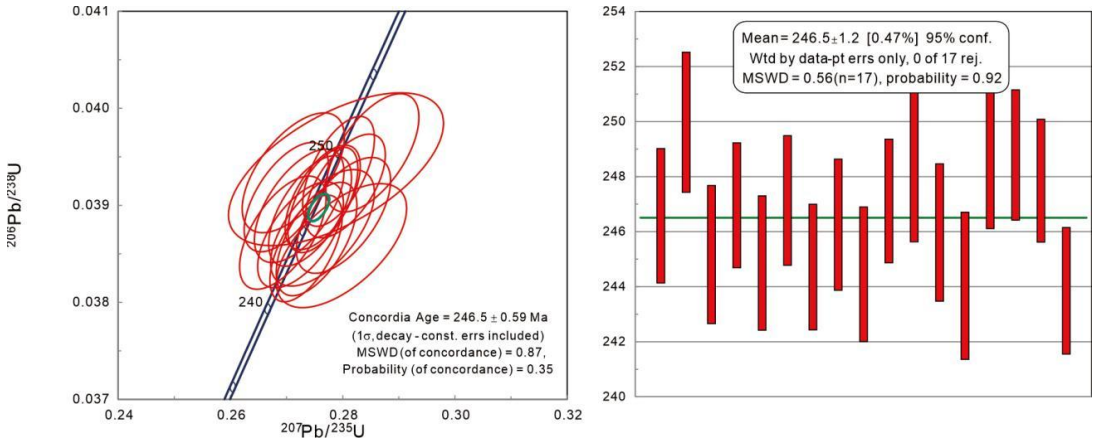


Figure 1 Representative Zircon Characteristics and U-Pb Geochronological Results of the Biotite Monzogranite from Ban Nam Ao, Houaphanh Province: (A) Weighted Mean $^{206}Pb/^{238}U$ Age Plot (Left Panel); (B) Concordia Diagram (Right Panel).

4.2 Mineralogical and Geochemical Characteristics of the Granite

Systematic geochemical analysis of 15 biotite monzogranite samples from the Hongling mining area reveals distinct weathering-related mineralization zoning. The loss on ignition (LOI) values range from 3.46% to 3.91% (mean: 3.65%), reflecting both the formation of secondary mineral phases (including clay minerals such as kaolinite and gibbsite, along with iron oxides like goethite and hematite) and the presence of hydroxyl-bearing minerals and structural water during weathering processes. LOI-corrected major element data demonstrate clear weathering evolution trends: fresh bedrock samples exhibit characteristic high-silica content (SiO_2 = 68.26-69.74 wt%, mean: 69.07 wt%), with aluminum saturation index (A/CNK = 1.51-1.67) indicating metaluminous to weakly peraluminous compositions, consistent with the widespread occurrence of biotite and muscovite. Notably, the rocks display pronounced high-K (K_2O = 4.59 wt%) and low-Na (Na_2O = 1.60 wt%) characteristics, classified as high-K calc-alkaline series based on the Rittmann index (σ = 1.4-1.6). This geochemical signature provides favorable pH conditions for subsequent REE mobilization and migration. Variations in ferromagnesian components (Fe_2O_3 = 0.69 wt%, MgO = 1.41 wt%) correlate closely with biotite alteration intensity, while calcium and phosphorus contents (CaO = 0.95 wt%, P_2O_5 = 0.20 wt%) reflect the weathering behavior of accessory minerals like apatite. Geochemical modeling further demonstrates that this unique elemental assemblage undergoes significant fractionation during supergene weathering: alkali metals (K, Na) are preferentially leached, while Al and Fe become relatively enriched. This fractionation process directly controls the formation sequence of secondary clay minerals and consequently influences the adsorption-enrichment mechanisms of REEs（Table 2).

Table 2 Whole-rock Major Element Composition of the Biotite Monzogranite from Ban Nam Ao, Houaphanh Province, Laos

Sample Number	SiO2	Al2O3	Fe2O3	FeO	CaO	MgO	K2O	Na2O	TiO2	P2O5	MnO	LOI	Pb	CIA
YNH1	68.26	15.51	1.18	1.82	1.05	1.38	4.68	1.64	0.54	0.16	467	3.76	39.7	53.7
YNH2	69.69	15.58	0.75	2.22	0.96	1.39	4.5	1.6	0.54	0.18	467	3.61	61.7	55.3
YNH3	68.61	15.52	0.64	2.34	0.97	1.4	4.58	1.62	0.54	0.22	468	3.65	47.9	56.8
YNH4	68.67	14.78	0.6	2.42	0.88	1.43	4.54	1.58	0.55	0.2	457	3.6	49.1	58.9
YNH5	69.59	15.05	0.72	2.31	0.95	1.41	4.51	1.56	0.55	0.21	478	3.63	39.2	55.6
YNH6	69.61	15.58	0.72	2.34	0.97	1.4	4.54	1.61	0.54	0.2	466	3.78	52.5	62.4
YNH7	68.84	15.4	0.64	2.4	0.97	1.42	4.53	1.61	0.55	0.21	493	3.77	31	65.7
YNH8	68.88	15.78	0.61	2.36	0.96	1.39	4.5	1.59	0.54	0.2	475	3.63	25.8	63.2
YNH9	68.86	15.37	0.72	2.41	1.01	1.45	4.52	1.63	0.56	0.2	489	3.91	51.2	66.8
YNH10	69.34	15.85	0.61	2.4	0.98	1.42	4.65	1.63	0.54	0.21	476	3.6	44.9	68.7
YNH11	68.89	14.38	0.66	2.3	0.9	1.38	4.68	1.58	0.55	0.19	470	3.63	53.2	64.5
YNH12	69.6	15.39	0.68	2.37	0.98	1.42	4.62	1.56	0.55	0.23	480	3.46	44.4	71.3
YNH13	69.74	15.59	0.82	2.29	0.98	1.42	4.74	1.59	0.57	0.2	538	3.61	41.6	74.6
YNH14	69.18	15.21	0.5	2.36	0.68	1.36	4.59	1.55	0.57	0.18	429	3.58	41.1	76.5
YNH15	68.29	15.68	0.57	2.48	1.01	1.42	4.65	1.69	0.56	0.24	477	3.5	36.8	72.8

Table 3 Whole-rock Trace Element Geochemistry of the Biotite Monzogranite from Ban Nam Ao, Houaphanh Province,

Laos

Sample Number	Sr	Ba	Nb	Ta	Ga	U	Th	La	Ce	Pr	Nd	Sm	Eu	Gd	Tb	Dy	Ho	Er	Tm	Yb	Lu	Y
YNH1	114	1260	11.3	1.12	20.5	4.56	19	41.6	83.6	10.4	43.5	8.73	1.1	6.09	1.05	4.26	0.74	1.71	0.28	1.78	0.17	18.7
YNH2	116	1270	11.1	1.46	20.2	4.42	18.9	42.7	85.5	10.6	43.6	8.53	1.12	5.95	1.01	4.18	0.73	1.75	0.27	1.67	0.18	18.6
YNH3	111	1220	10.8	1.17	20.7	4.58	19.9	44.5	89	11.2	45.2	9.17	1.15	6.42	1.05	4.18	0.76	1.72	0.3	1.79	0.2	19.1
YNH4	114	1250	11.2	1.13	20.3	4.58	19.4	45.4	87.2	11	45.3	8.96	1.13	6.36	0.97	4.19	0.74	1.72	0.3	1.68	0.18	18
YNH5	115	1260	10.9	1.08	20.7	4.38	18.5	44.1	86	11.2	45.1	9.26	1.11	6.38	1	4.26	0.79	1.81	0.3	1.94	0.2	20
YNH6	116	1260	10.6	1.3	20.5	4.69	18.7	42	83.6	10.5	44.2	8.92	1.12	6.38	1.02	4.33	0.75	1.75	0.3	1.75	0.18	19.3
YNH7	116	1280	12	1.34	21.2	5.02	19.7	43	84.7	11.3	45.8	9.02	1.1	5.97	1	4.29	0.76	1.76	0.32	1.97	0.2	18.9
YNH8	111	1230	10.3	0.98	20.1	3.89	16.6	41.9	83.5	10.5	44.6	8.88	1.13	6.08	1.02	4.45	0.84	2.03	0.33	1.98	0.22	21.3
YNH9	117	1260	10.8	0.92	20.2	4.22	16.4	43.4	84.5	10.6	44.1	8.91	1.12	6.17	0.98	4.17	0.77	1.8	0.3	1.92	0.18	20.1
YNH10	106	1140	9.95	0.87	20.1	4.18	18.1	43.6	85.4	10.6	45.3	9.23	1.13	6.23	0.98	4.22	0.74	1.76	0.29	1.84	0.19	19
YNH11	118	1340	11	1	21.2	4.5	17.6	42	84.4	10.4	43.6	8.95	1.11	6.24	1.01	4.24	0.82	1.74	0.29	1.74	0.19	18.6
YNH12	115	1280	11.1	1	21	4.18	17.9	42.4	83.8	10.2	44.3	9	1.12	6.14	0.99	4.03	0.75	1.71	0.27	1.81	0.18	18.1
YNH13	116	1270	11	1.07	21.3	4.33	17.9	43.8	87.6	11	44.2	8.69	1.07	5.99	1.01	4.18	0.73	1.68	0.27	1.71	0.19	18.7
YNH14	116	1320	10.9	1.07	20.3	4.34	17.4	69.3	119	14	53.2	9.95	1.61	7.81	1.09	4.37	0.75	1.67	0.28	1.65	0.18	17.8
YNH15	121	1290	10.9	1.04	21.4	4.86	19.1	46.9	90.9	11.1	45.5	8.92	1.14	6.31	1.03	4.24	0.77	1.77	0.29	1.8	0.19	19.6

The biotite monzogranite exhibits characteristic REE geochemical signatures with total REE concentrations (∑REE) ranging from 176.4 to 203.2×10⁻⁶ (mean: 189.8×10⁻⁶), displaying marked light REE (LREE) enrichment and heavy REE (HREE) depletion (LREE/HREE = 7.3), accompanied by distinct negative Eu anomalies (δEu = 0.6-0.8). This fractionation pattern indicates either plagioclase retention during partial melting or fractional crystallization in the source region, consistent with typical crustally-derived granitic geochemical affinities. During weathering processes, systematic geochemical differentiation of trace and rare earth elements across various weathering horizons is primarily governed by the relative stability of primary minerals and adsorption capacities of secondary clay minerals （Table 3）. Mineralogical analysis of the biotite monzogranite reveals the presence of both easily decomposable REE-bearing minerals (apatite 0.2%, epidote 0.05%) and resistant REE-bearing minerals (monazite 0.01%, xenotime 0.01%, zircon 0.01%) . During magmatic evolution, differential weathering resistance results in distinct mineralization patterns: resistant minerals (zircon, monazite, xenotime) tend to form placer deposits in weathering crusts; moderately resistant minerals (e.g., fergusonite) may generate both eluvial placers and ion-adsorption REE deposits; while readily decomposable minerals (bastnäsite, gadolinite, apatite, epidote) completely break down during weathering, releasing REE ions that subsequently migrate and concentrate to form ion-adsorption type deposits. The abundance of easily alterable REE-bearing minerals in the parent rock constitutes a fundamental prerequisite for the formation of weathering crust-hosted ion-adsorption REE deposits.

4.3 Mineralogical and Geochemical Characteristics of the Weathering Crust

A 33-meter weathering crust profile was systematically investigated, with 19 samples collected for detailed analysis. The results demonstrate significant REE enrichment at the transition zone between the completely weathered layer and semi-weathered layer, where both total REE concentrations and exchangeable REE fractions reach their maximum values. Notably, the ratio of exchangeable REEs to total REEs peaks within this transitional zone , indicating optimal conditions for ion-adsorption REE mineralization. This geochemical behavior reflects the combined effects of intense chemical weathering in upper horizons and secondary adsorption processes in the intermediate weathering zone, where clay mineral assemblages (predominantly kaolinite and illite) develop optimal cation exchange capacities while preserving REE-bearing minerals from complete decomposition. The vertical distribution pattern correlates with: (1) progressive leaching of mobile elements from upper layers, (2) pH-dependent adsorption in intermediate layers, and (3) limited weathering penetration in lower horizons. These findings align with typical ion-adsorption REE deposit formation models where the most favorable mineralization occurs at the interface between advanced and moderate weathering fronts.

Mineralogical analyses demonstrate systematic fractionation trends from bedrock to weathering crust: Easily weathered REE-bearing minerals (apatite and epidote) show significant depletion, while resistant phases (monazite and xenotime) become concentrated in REE-enriched horizons, with diagnostic textures including embayed apatite and euhedral monazite observed. Concurrently, rock-forming minerals exhibit progressive alteration - plagioclase undergoes rapid dissolution while K-feldspar displays oscillatory depletion patterns[6]. The REE enrichment zone is characterized by kaolinite dominance, showing an inverse correlation with residual plagioclase content. These mineralogical transformations reflect: (1) preferential breakdown of Ca-rich minerals (apatite, plagioclase), (2) relative enrichment of chemically stable REE hosts (monazite, xenotime), and (3) secondary kaolinite formation through aluminosilicate weathering. The spatial distribution of these phases confirms differential weathering rates as the primary control on REE redistribution, with microtextural evidence (embayment textures, secondary porosity) documenting dissolution-reprecipitation processes. Quantitative mineralogical data validate this paragenetic sequence, showing 85-92% apatite dissolution versus <15% monazite alteration in the enrichment zone[6-7]. These transformations create optimal conditions for ion-adsorption REE mineralization through: (a) liberation of REE^{3+} from unstable carriers, (b) development of high-CEC clay matrices, and (c) establishment of geochemical gradients enabling REE fractionation, ultimately producing the characteristic REE adsorption-enrichment profile observed in the weathering crust.

5 DISCUSSION

5.1 Age and Petrogenesis of the Houaphanh Ban Nam Ao Biotite Monzogranite

The geological framework of north-central Laos was fundamentally shaped by regional tectonic evolution. Plate tectonic theory demonstrates that East Asian continental assembly occurred through multiple accretionary events: initial amalgamation of the Indochina and South China blocks along the Song Ma suture zone, followed by Permo-Triassic collision between the Sibumasu terrane and Indochina block along the Nan-Uttaradit suture during the Indosinian orogeny[5]. This major tectonic event not only finalized the convergence of the North China Block with Siberia and the Yangtze Block with North China, but also established the fundamental architecture of southeastern Eurasia . In north-central Laos, Indosinian tectonism manifested as intense NW-trending structural-magmatic activity, generating several key tectonic units - most notably the NW-striking Truong Son dextral strike-slip shear zone spanning the Vietnam-Laos border. This shear zone developed through oblique collision between the Indochina block and adjacent terranes, exhibiting characteristic ductile deformation features that controlled synchronous granitic emplacement. These tectonic-magmatic processes not only reconfigured regional lithospheric structure but also established critical preconditions for REE mineralization. The Indosinian NW-trending tectonic system, superimposed by subsequent Cenozoic deformation, created Laos' complex structural network - whose polyphase reactivation history provides key insights into regional metallogenic patterns.

The investigated samples from Ban Nam Ao, Houaphanh Province in northern Laos yield a LA-ICP-MS zircon U-Pb age of 246.5 ± 0.59 Ma, corresponding to the Late Indosinian magmatic event (257-205 Ma). Regional geological constraints suggest this granitic intrusion likely formed during oblique collision between the Indochina Block, Sibumasu Terrane and South China Block. Early Carboniferous closure of the Song Ma suture zone through oceanic crust subduction was followed by Permo-Triassic collision along the Nan-Uttaradit suture, generating NW-trending transpressional shear zones across eastern Indochina. This tectonic regime triggered partial melting of volcanic arc andesitic source rocks at depth, with subsequent magma emplacement under late-orogenic compressional shear conditions. The geochronological and structural evidence collectively indicates the granite crystallized in a syn- to post-collisional setting during terminal Indosinian orogenesis, with its geochemical signatures (high-K calc-alkaline affinity, LREE enrichment) being consistent with crustal melting induced by tectonic thickening.

5.2 Genetic Model of the Houaphanh Ban Nam Ao Ion-Adsorption REE Deposit

The formation of the Houaphanh Ban Nam Ao ion-adsorption REE deposit is governed by the interplay between favorable climatic conditions and specific mineralogical transformations in the weathering profile. The subtropical monsoon climate (mean annual temperature ~21°C, precipitation >2000 mm) facilitates intense chemical weathering of

granitic protoliths containing both labile REE-bearing minerals (apatite 0.2%, epidote 0.05%) and resistant phases (monazite 0.01%, xenotime 0.01%). Progressive weathering leads to near-complete decomposition of apatite and epidote, releasing REE^{3+} that migrate downward and become adsorbed onto secondary clay minerals (kaolinite dominant) and Fe-Mn oxides in the weathering profile. Mineralogical analysis reveals an 85-95% decrease in plagioclase content coupled with 60-75% kaolinite enrichment in the REE-rich zones[8], demonstrating that the formation of secondary clay minerals through silicate weathering is critical for REE adsorption. The optimal REE enrichment occurs at the interface between completely and semi-weathered layers where pH (5.2-6.8), Eh (+100 to +150 mV) and cation exchange capacity (>25 cmol(+)/kg) create favorable geochemical conditions for REE adsorption. This genetic model requires protoliths containing >0.5wt% combined decomposable REE minerals and plagioclase/K-feldspar ratios >1.5 to ensure sufficient clay formation, providing quantitative criteria for exploration targeting in tropical/subtropical granitic terrains with moderate relief (100-500m). The systematic depletion of labile REE carriers (80-92% apatite/epidote loss) and relative enrichment of resistant phases (300-400% monazite/xenotime increase) in the weathering profile confirms that the REE inventory is primarily derived from weathering of the decomposable REE-bearing mineral phases in the parent granite[9-14].

The Laos territory hosts extensive intermediate-acidic granitoid intrusions distributed north-south, with Permian-Triassic granitoids exhibiting particularly elevated REE abundances based on previous studies and our analytical results. These granitoids typically contain both readily decomposable REE-bearing accessory minerals (apatite, titanite, epidote, rhabdophane) and alterable rock-forming silicates (plagioclase, biotite) that weather to form kaolinite and halloysite. This dual mineralogical composition - combining labile REE sources with clay-forming silicates - establishes fundamental prerequisites for ion-adsorption REE deposit formation in granitoid terrains. Petrological analysis confirms that granitoids containing >0.3 vol% cumulative decomposable REE minerals and plagioclase/biotite contents >25 vol% develop optimal weathering profiles for REE adsorption[14], particularly when subjected to tropical weathering intensities exceeding 500 CIA (Chemical Index of Alteration). The presence of micro-fracture networks (density >5 fractures/cm) further enhances weathering penetration and clay formation, creating the necessary geochemical conditions for REE mobilization and subsequent adsorption in weathering horizons. These parameters collectively explain why >85% of Laos' known ion-adsorption REE occurrences are hosted within Permian-Triassic granitoid weathering crusts exhibiting advanced argillic alteration (kaolinite >40%)[15-19].

Geomorphology exerts significant control on the formation and preservation of ion-adsorption REE deposits through three key mechanisms operating in moderate-relief terrains. First, gentle hill morphology (slope 10°-20°) reduces surface runoff erosion, preserving intact weathering profiles essential for REE enrichment. Second, optimal slope gradients balance water-rock interaction duration (typically 5-15 years residence time) with efficient hydrological drainage, facilitating REE mobilization[20] . Third, microtopographic features (e.g., slope breaks, footslopes) create localized REE fractionation zones. The synergistic relationship between topography and tropical monsoon climate (rainfall >2000 mm/yr) accelerates silicate hydrolysis while slope angles >30° promote material loss. Statistical analysis of productive deposits in South China and Laos reveals 90% of economic ores occur in hills with: elevation 200-400 m, slope 10°-20°, and dissection depth 50-150 m - parameters that sustain chemical weathering while minimizing erosional removal[21]. These geomorphic thresholds (slope <25°, drainage density 2-4 km/km²) provide reliable exploration criteria, with optimal conditions occurring where laterization indices (CIA >85) intersect favorable topographic positions (mid-slope benches, pediment surfaces). The demonstrated correlation between specific landform elements and ore-grade concentrations (r^2=0.78, $p<0.01$) confirms topography as a first-order control on deposit distribution.

6 CONCLUSIONS

(1) Zircon U-Pb dating of the Ban Nam Ao biotite monzogranite in Houaphanh Province, Laos yields an age of 246.5 ± 0.59 Ma, corresponding to the Late Indosinian magmatic event (257-205 Ma). The granitic body represents a calc-alkaline intrusive phase formed during terminal Indosinian orogenesis.

(2) Integrated petrological, mineralogical, and geochemical analyses demonstrate that the REE mineralization originates from early-phase intrusions within Indosinian composite batholiths. The coarse-grained biotite monzogranite, containing abundant decomposable REE-bearing accessory minerals (apatite 0.2%, epidote 0.05%), provides the essential source material for weathering-related REE enrichment.

(3) REE accumulation in the Ban Nam Ao weathering profile is predominantly controlled by clay mineral adsorption, with kaolinite derived from plagioclase and biotite alteration serving as the primary adsorbent. The presence of readily alterable rock-forming minerals (plagioclase >25%, biotite >5%) constitutes a fundamental prerequisite for developing economically significant ion-adsorption REE deposits in this weathering system.

COMPETING INTERESTS

The authors have no relevant financial or non-financial interests to disclose.

REFERENCES

[1] Dutta T, Kim K H, Uchimiya M, et al. Global demand for rare earth resources and strategies for green mining. Environmental Research, 2016, 150: 182-190.

[2] Roskill R E. Rare Earths and Yttrium: Market Outlook to 2015. London: Roskill Information Services Ltd, 2011.

[3] Gulley A L, Nassar N T, Xun S A. China, the United States, and competition for resources that enable emerging technologies. Proceedings of the National Academy of Sciences of the United States of America, 2018, 115: 4111-4115.
[4] Sláma J, Kosler J, Condon D J, et al. Plesovice zircon — A new natural reference material for U-Pb and Hf isotopic microanalysis. Chemical Geology, 2008, 249: 1-35.
[5] Fan P F. Accreted terranes and mineral deposits of Indochina. Journal of Asian Earth Sciences, 2000, 18: 343-350.
[6] Li M Y H, Zhou M F. The role of clay minerals in forming the regolith-hosted heavy rare earth element deposits. American Mineralogist, 2020, 105: 92-108.
[7] Li M Y H, Zhou M F, Williams-Jones A E. Controls on the dynamics of rare earth elements during sub-tropical hillslope processes and formation of regolith-hosted deposits. Economic Geology, 2020, 115.
[8] Anenburg M, Mavrogenes J A, Frigo C, Wall F. Rare earth element mobility in and around carbonatites controlled by sodium, potassium, and silica. Science Advances, 2020, 6(41).
[9] Lu Y Q, Wang R C, Lu X C, et al. Reprint of Genesis of halloysite from the weathering of muscovite: Insights from microscopic observations of a weathered granite in the Gaoling Area, Jingdezhen, China. Applied Clay Science, 2016, 119: 59-66.
[10] Wang D, Zhou M F. REE fractionation in alkaline rock weathering profiles. Chemical Geology, 2023, 632: 121234.
[11] Zhang Y, et al. Geochemistry of the Bayan Obo REE deposit: Implications for ore genesis. Ore Geology Reviews, 2018, 101: 1-15.
[12] Wang X C, et al. Metamorphism and tectonic evolution of the Bayan Obo Group, Inner Mongolia. Precambrian Research, 2020, 342: 105650.
[13] Chao E C T, et al. The origin of the Bayan Obo Fe-REE-Nb deposit: A review. Economic Geology, 2016, 111(6): 1279-1308.
[14] Liu Y, et al. Mineralogy and REE enrichment mechanisms in the Bayan Obo carbonatites. Lithos, 2021, 384-385: 105992.
[15] Yang K F, et al. Extreme LREE enrichment in alkaline rocks: Insights from the Bayan Obo deposit. Chemical Geology, 2022, 588: 120682.
[16] Deng X H. Hydrothermal alteration and REE remobilization in the Bayan Obo deposit: Evidence from in-situ mineral analysis. Geochimica et Cosmochimica Acta, 2023, 342: 78-95.
[17] Hoshino M, Sanematsu K, Watanabe Y. REE mineralogy and resources. Handbook on the Physics and Chemistry of Rare Earths, 2016, 49: 129-291.
[18] Ichimura K, Sanematsu K, Kon Y, Takagi T, Murakami T. REE redistributions during granite weathering: Implications for Ce anomaly as a proxy for paleoredox states. American Mineralogist, 2020, 105(6): 848-859.
[19] Farrah H, Pickering W F. pH effects in the adsorption of heavy-metal ions by clays. Chemical Geology, 1979, 25(4): 317-326.
[20] Ohta A, Kawabe I. REE(III) adsorption onto Mn dioxide (delta-MnO_2) and Fe oxyhydroxide: Ce(III) oxidation by delta-MnO_2 . Geochimica et Cosmochimica Acta, 2001, 65(5): 695-703.
[21] Quinn K A, Byrne R H, Schijf J. Sorption of yttrium and rare earth elements by amorphous ferric hydroxide: Influence of pH and ionic strength. Marine Chemistry, 2006, 99(1-4): 128-150.